complexation/fusion behavior of these same carboranes.[6,7,11,12] Thus, the more sterically hindered species, which exhibit slow deprotonation, similarly are the most sluggish toward formation of $(RR'C_2B_4H_4)_2FeH_2$ complexes and conversion of the latter to $R_2R'_2C_4B_8H_8$. Indeed, when R and R' are both very large (e.g., indenylmethyl, fluorenylmethyl, or $(CO)_3CrPhCH_2$), fusion fails to occur at all.[12] This correlation further strengthens the rationale of a mainly steric role for the substituents in the deprotonation process.

Other aspects of the deprotonation reaction, including the consequences of B substitution on the basal ring and the kinetics of the homogeneous reactions with alkyllithium reagents, have not been addressed in this study but are worthy of investigation and may be examined in future work.

Acknowledgment. This work was supported in part by the National Science Foundation (Grant No. CHE 84-19401). We thank Henry Boyter, Jr., for the rate data on $Ph_2C_2B_4H_6$ and Professor Jack Steehler for assistance in data plotting.

Supplementary Material Available: Description of the method employed for error calculations and tables of observed P_{H_2} vs. time for deprotonation rate measurements (46 pages). Ordering information is given on any current masthead page.

Phases in the System XeF_2/XeF_5AsF_6 and Structural and Vibrational Evidence for the Following Ionization Pathway: $XeF_2 \rightarrow XeF^+ + F^-$

Boris Žemva,[1a,b] Adolf Jesih,[1b] David H. Templeton,[1a] Allan Zalkin,[1a] Anthony K. Cheetham,[1a,c] and Neil Bartlett*[1a]

Contribution from the Materials and Chemical Sciences Division, Lawrence Berkeley Laboratory and Department of Chemistry, University of California, Berkeley, California 94720, "Jožef Stefan" Institute, "Edvard Kardelj" University, 61000 Ljubljana, Yugoslavia, and Chemical Crystallography Laboratory, University of Oxford, Oxford OX1 3PD, England.
Received June 1, 1987

Abstract: A fusion temperature versus composition curve has been obtained for the system XeF_2/XeF_5AsF_6. X-ray single-crystal and powder diffraction methods have been used in combination with Raman spectroscopy to characterize the various phases that are formed. The fusion temperature/composition curve indicates compound formation at XeF_2 to XeF_5AsF_6 ratios (fusion temperature in parentheses): 1:2 (89.5 °C), 2:1 (59.5 °C), and 3:1 (74.0 °C). Other simple integer combinations are also suggested at the ratios 1:1 (56.5 °C) and 3:2 (56.0 °C). The high viscosity of the 1:2 melt, at its melting point, suggests that the polymeric fluorine-bridged structure of the solid largely persists in the early liquid phase. In contrast the melts of the 1:1 and 2:1 are distinctly more mobile and probably consist of the monomeric formula unit species, which are characteristic of the crystalline phases. The deepest eutectic occurs at 49 °C, with 57 mol % XeF_2. This easily supercools to ambient temperatures. Another well-defined eutectic occurs at 56 °C with 71.0 mol % XeF_2. $XeF_2{\cdot}2(XeF_5AsF_6)$ is monoclinic, $P2_1/n$, with a = 12.033 (6) Å, b = 7.024 (4) Å, c = 10.940 (5) Å, β = 95.43 (5)°, Z = 2, and D_x = 3.61 g cm^{-3}. The linear symmetrical XeF_2 species [Xe–F = 2.0 (1) Å] are coordinated via their F ligands to two equivalent XeF_5^+ ions [F···Xe(VI) = 2.76 (2) Å and angle Xe(II)—F···Xe(VI) = 139.4 (6)°]. The XeF_5^+ ions are also bridge bonded to two AsF_6^- ions [Xe(VI)···F = 2.66 (1) and 2.74 (1) Å], the anion thus being coordinated to two cations, a three-dimensional polymer being thereby formed. $XeF_2{\cdot}XeF_5AsF_6$ is monoclinic, $P2_1/n$, with a = 9.159 (4) Å, b = 10.158 (5) Å, c = 12.401 (6) Å, β = 106.66 (5)°, z = 4, and D_x = 3.51 g cm^{-3}. The structural unit is the formula unit $XeF_2{\cdot}XeF_5AsF_6$. These units are not interconnected. The XeF_2 molecule is approximately linear [F–Xe–F = 178.1 (5)°], but the F ligand, which makes a bridge bond to the XeF_5^+, is elongated [Xe–F = 2.06 (1) Å] and the other XeF bond is appreciably shortened [Xe–F = 1.97 (1) Å]. The bridge bond to the XeF_5^+ from the XeF_2 is short [F(Xe)···Xe(VI) = 2.47 (1) Å] as is that from the AsF_6^- ion [F(As)···Xe(VI) = 2.59 (1) Å]. These two bridging F ligands are coplanar with the Xe(VI) atom and the axial fluorine of the XeF_5^+. The symmetry of the cation and its bridging ligands is roughly C_{2v}. $2XeF_2{\cdot}XeF_5AsF_6$ is monoclinic, $P2_1/a$, with a = 12.295 (9) Å, b = 8.275 (6) Å, c = 13.455 (7) Å, β = 95.67 (4)°, z = 4, and D_x = 3.67 g cm^{-3}. As in the 1:1 compound, the formula unit is the structural unit and these units are not interconnected. The XeF_2 molecules are again nearly linear [F–Xe–F = 177 (1) and 179 (1)°] and the Xe–F bond involving F bridging to the cation is in each case elongated [F···Xe(VI) = 2.05 (1) Å for each] and the nonbridging Xe–F is shortened slightly [1.99 (1) and 2.01 (1) Å]. These XeF_2 interactions with XeF_5^+ are evidently weaker than in the 1:1 compound, the F(Xe)···Xe(VI) bridging distances in this case being 2.53 (1) and 2.54 (1) Å. The bridging F ligands from the two attached XeF_2 molecules are coplanar with the axial Xe–F unit of the cation. This indicates that the closest F ligand of the AsF_6^- to the XeF_5^+, at 2.94 (1) Å, is interacting only weakly with the cation. Differences in the coordination number of the XeF_5^+ cation in these complexes account for the polymeric or nonpolymeric nature of the complexes. Such differences are determined by the extent of ionization of the XeF_2 species. The observed, essentially linear, distortions of XeF_2 are interpreted as points on the ionization pathway $XeF_2 \rightarrow XeF^+ + F^-$. From the force constants, and associated interatomic distances, the isolated XeF^+ ion is predicted to have a bond length of ~1.92 Å and a force constant of ≤4.48 mdyn/Å.

From theoretical considerations Jortner, Rice, and Wilson in 1963 concluded[2] that the bond ionicity in xenon difluoride was approximately $F^{-0.5}$–Xe^{1+}–$F^{-0.5}$ and on this basis they predicted that the enthalpy of sublimation, $\Delta H°_{sub}$, should be 13.3 kcal mol^{-1}. This derived largely from the lattice energy contributed by the semi-ionic lattice. Subsequently Schreiner and his co-workers[3] determined the sublimation enthalpy by experiment and found $\Delta H°_{sub}$ = 13.2 ± 0.2 kcal mol^{-1}. This gave striking support for the proposed high bond polarity in the molecule. Similar high

(1) (a) University of California. (b) "Edvard Kardelj" University. (c) University of Oxford.

(2) Jortner, J.; Rice, S. A.; Wilson, E. Guy *Chem. Phys.* **1963**, *38*, 2302. Jortner, J.; Wilson, E. Guy; Rice, S. A. *J. Am. Chem. Soc.* **1963**, *85*, 814.

(3) Schreiner, F.; McDonald, G. N.; Chernick, C. L. *J. Phys. Chem.* **1968**, *72*, 1162.

0002-7863/87/1509-7420$01.50/0

bond ionicities have been indicated from ESCA[4] and Mössbauer[5] spectroscopy for other xenon fluorides and oxyfluorides and for the halogen fluorides from ESCA.[6] The semi-ionic bonding of these molecules provides the lattice energy which stabilizes molecular adducts such as $XeF_2 \cdot XeF_4$,[7] $XeF_2 \cdot IF_5$,[8] and $XeF_2 \cdot XeOF_4$.[9] In these adducts the individual molecular species have essentially the same size and shape as in a crystal of the pure component. In all of them the F ligands of one molecule show maximum avoidance of other F ligands and are directed toward the central atom (positively charged) of the other molecule. This provides the best lattice energy for the semi-ionic assembly.

The isoelectronic relationship and near identity of shape of XeF_5^+ to IF_5 and $XeOF_4$ suggested that XeF_2 might also make adducts with that ion. It was, however, recognized from the work of Berkowitz and his co-workers[10] that the enthalpy of ionization, $\Delta H°(XeF_{x(g)} \rightarrow XeF_{(g)x-1} + F^-_{(g)})$, of XeF_2 (9.45 eV) was only slightly greater than that of XeF_6 (9.24 eV). This small difference is offset somewhat by the slightly more favorable lattice enthalpy for a XeF^+ salt when compared with its XeF_5^+ relative. This is because of the smaller size of the former cation. The possibility therefore existed for the acid–base interactions

$$XeF_2 + XeF_5^+ \rightarrow XeF^+ + XeF_6 \qquad (1)$$

Adducts of XeF_2 with XeF_5 salts were indeed found[9] and Raman spectroscopy (and particularly the intense totally symmetric stretching vibration at 496 cm^{-1} characteristic[11] of XeF_2) indicated that in the adduct $XeF_2 \cdot 2(XeF_5AsF_6)$ the XeF_2 molecule was indistinguishable from that in crystalline XeF_2 itself and therefore was effectively of $D_{\infty h}$ symmetry. Raman spectroscopy showed that the symmetric stretching vibration of XeF_2 was not present in the 1:1 adduct, $XeF_2 \cdot XeF_5AsF_6$. But two bands, at 557 and 429 cm^{-1} (average 494 cm^{-1}), were identified as XeF stretching modes of what was conjectured to be a linearly distorted XeF_2 molecule. This suggested that the XeF_2 molecule in this instance was interacting strongly with the XeF_5^+ as though on the reaction pathway for eq 1. Other adducts between XeF_2 and XeF_5AsF_6 appeared to be possible but no others were specifically identified at that time.

The low melting point observed for the 1:1 adduct (~57 °C) relative to the separate components (XeF_2, 129 °C; XeF_5AsF_6, 132 °C) and the hint of even lower melting materials, taken together with the observation that the Raman spectra at the melting points are similar to those of the crystalline solids, suggested that these and other $XeF_2 \cdot n(XeF_5MF_6)$ salts could provide low-temperature melts, which would be highly resistent to further oxidation. These are of particular interest as potential sources of MF_6 via anodic oxidation of the MF_6^- salts.

In order to obtain a firmer understanding of the factors that determine adduct formation and also to investigate the possibility of lower fusion temperatures, the phase diagram for the XeF_2/XeF_5AsF_6 system has been broadly surveyed. Representative structures (for the XeF_2:XeF_5AsF_6 ratios 1:2, 1:1, and 2:1) have been carried out with X-ray single-crystal diffraction methods. Structural changes and relationships have been otherwise followed by X-ray powder photography and Raman spectroscopy. This paper describes the main findings.

Experimental Section

Melting Point Measurements in the System XeF_2/XeF_5AsF_6. Materials. XeF_2 and XeF_5AsF_6 were prepared as previously described.[12,13]

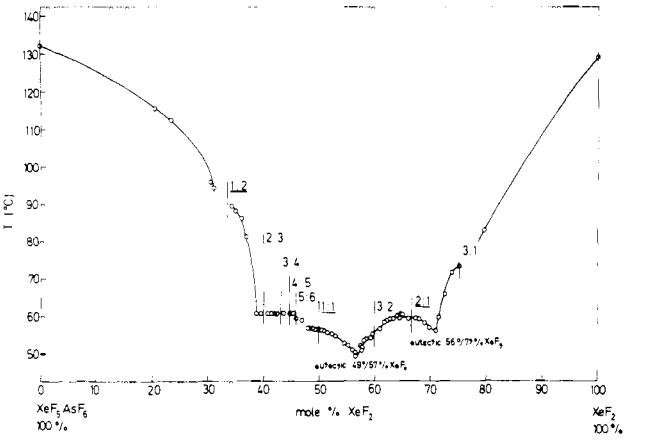

Figure 1. Fusion temperature composition curve for XeF_2/XeF_5AsF_6.

All handling of the solids was carried out in the dry-nitrogen atmosphere of a Vacuum Atmospheres Corp. Drilab or in another drybox of comparable dryness.

Apparatus. A thin-walled quartz ampule of ~10 cm^3 capacity joined to a nickel needle valve via Teflon-gasketed compression fittings was used to contain the samples to be melted. A Teflon-coated stirrer bar was placed in the ampule with the sample.

Sample Preparation. Each compound (XeF_2 and XeF_5AsF_6) was separately weighed into the quartz ampule in the drybox. Each quantity was roughly determined with a balance housed in the drybox and subsequently measured with a balance outside the box with a precision of ±0.1 mg. The total quantity of adduct prepared was in each case 12 to 15 mmol. After the more precise weighing (which provided the composition) the entire capsule volume was immersed in hot water, to a point beyond the valve seat, so that the sample melted completely. The melt was then homogenized by stirring and subsequently cooled to solidify the sample. A melting point determination was carried out on that solidified sample. By removing XeF_2 under vacuum (the loss being assessed gravimetrically) the composition of the material in the ampule was progressively enriched in $XeF_5 \cdot AsF_6$. After each such adjustment in composition the residual material was homogenized by stirring of the melt. A melting point was carried out on this solidified, homogenized material. Only 4 to 5 adjustments in composition of this kind were made, then a fresh mixture of XeF_2 and XeF_5AsF_6 was prepared so as to provide a compositional overlap with the previous one.

Measurements. A thermostat bath containing water or glycerine (at temperatures above 95 °C) was used in the melting point determinations. The temperature was regulated to ±0.02 °C. A calibrated thermometer was used. The melting point was taken as the temperature at which the last crystals of solid became liquid or at which turbidity cleared.

Raman spectra were typically obtained from samples sealed in thin-walled quartz capillaries of ~1 mm diameter. Spectra were recorded with a Spex 1401 double monochromator with either krypton or argon ion laser radiation.

X-ray Structure Determinations. Crystals of the three compositions reported in this paper were grown in 0.3-mm evacuated quartz capillaries. The details of the crystal shape, color, and size are recorded in Table I. The crystals were mounted on a Picker FACS-I automated diffractometer equipped with a scintillation counter, a graphite monochromator, and a Mo X-ray tube. The setting angles of 12 manually centered reflections [37° < 2θ < 51° for $XeF_2 \cdot XeF_5 \cdot AsF_6$ and 37° < 2θ < 41° for $XeF_2 \cdot 2(XeF_5 \cdot AsF_6)$] were used to determine the cell dimensions by a least-squares procedure; the setting angles of 3 reflections (0,8,0; 12,0,0; and 0,0,13) were used to determine the cell dimensions of $2XeF_2 \cdot XeF_5 \cdot AsF_6$; the results are shown in Table I. The intensity data were collected by using the θ–2θ scan, and most of the details of the data acquisition and results are shown in Table I. Crystal decay factors based on the variations of the standards reflections, absorption corrections,[14] and Lorentz–polarization corrections were applied to the intensity data. A perusal of the strong reflections after several least-squares refinements indicated an extinction correction would be warranted for the $XeF_2 \cdot 2(XeF_5 \cdot AsF_6)$ data only, and such a correction was made (see Table I).

(4) Caroll, T. X.; Shaw, R. W., Jr.; Thomas, T. D.; Kindle, C.; Bartlett, N. *J. Am. Chem. Soc.* **1974**, *96*, 1989.
(5) Perlow, G. J.; Perlow, M. R. *J. Chem. Phys.* **1968**, *48*, 955. Perlow, G. J.; Yoshida, H. *J. Chem. Phys.* **1968**, *48*, 1474.
(6) Shaw, R. W.; Carroll, T. X.; Thomas, T. D. *J. Am. Chem. Soc.* **1973**, *95*, 5870.
(7) Burns, J. H.; Ellison, R. D.; Levy, H. A. *Acta Crystallogr.* **1965**, *18*, 11.
(8) Sladky, F. O.; Bartlett, N. *J. Chem. Soc. A* **1969**, 2188. Jones, G. R.; Burbank, R. D.; Bartlett, N. *Inorg. Chem.* **1970**, *9*, 2264.
(9) Bartlett, N.; Wechsberg, M. *Z. Anorg. Allg. Chem.* **1971**, *385*, 5.
(10) Berkowitz, J.; Chuptka, W. A.; Guyon, P. M.; Holloway, J. H.; Spohr, R. *J. Phys. Chem.* **1971**, *75*, 1461.
(11) Smith, D. E. *Noble Gas Compounds*; Hyman, H. H., Ed.; The University of Chicago Press: Chicago and London, 1963; p 295.
(12) Williamson, S. M. *Inorg. Synth.* **1968**, *11*, 147. Lutar, K.; Šmalc, A.; Slivnik, J. *Vestn. Slov. Kem. Drus.* **1979**, *26*, 435.
(13) Bartlett, N.; DeBoer, B. G.; Hollander, F. J.; Sladky, F. O.; Templeton, D. H.; Zalkin, A. *Inorg. Chem.* **1974**, *13*, 780.
(14) Templeton, L. K.; Templeton, D. H. *Am. Cryst. Assocn. Proc.* **1973**, *Series 2, Vol. 1*, 143.

Table I. Summary of Crystal Data, Intensity Collection, and Least-Squares Processing

compd	$2XeF_2 \cdot XeF_5 \cdot AsF_6$	$XeF_2 \cdot XeF_5 \cdot AsF_6$	$XeF_2 \cdot 2(XeF_5 \cdot AsF_6)$
formula wt	753.80	580.50	999.71
a, Å	12.295 (9)	9.159 (4)	12.033 (6)
b, Å	8.275 (6)	10.158 (5)	7.024 (4)
c, Å	13.455 (7)	12.401 (6)	10.940 (5)
β, deg	95.67 (4)	106.66 (5)	95.43 (5)
V, Å^3	1362.2	1105.3	920.5
space group	$P2_1/a$	$P2_1/n$	$P2_1/n$
Z	4	4	2
density calcd, g/cm^3	3.67	3.51	3.61
color	colorless	colorless	colorless
crystal shape and size, mm	half-moon disk, ~0.04 thick × 0.20 radius	flat 6-sided plate, ~0.03 thick × ~0.10 across	acicular, 0.05 × 0.05 × 0.12
crystal vol, mm^3	0.0015	0.00025	0.00039
μ, cm^{-1}	99	92	93
absorption corr range	1.47–6.50	1.45–1.84	1.56–3.18
radiation, Å	Mo Kα (λ = 0.70930 and 0.71359), monochromatized from (002) face of mosaic graphite		
data collection method	θ–2θ scan (2°/min along 2θ)		
scan range, deg 2θ	1.5 plus Kα_1, Kα_2 divergence	1.5 plus Kα_1, Kα_2 divergence	1.4 plus Kα_1, Kα_2 divergence
T, °C	21 ± 1	21 ± 1	21 ± 1
bkgd count time, (total)	8 (no offset)	8 offset from scan limits by 1/4 deg	20
2θ limits, deg	4–50	4–50	4–45
no. of standards	3	3	3
freq of standards	after every 200th scan		
no. of scans (including standards)	5270	3758	2693
decay corr range	0.93–1.09	0.95–1.10	0.87–1.21
no. of unique data	2413	1607	1209
no. of data used in least squares	1694 ($F^2 > 1\sigma$)	824 ($F^2 > 3\sigma$)	640 ($F^2 > 3\sigma$)
extinction corr factor k, $F_{corr} = (1 + kI)F_{obsd}$	0	0	4.0×10^{-7}
ignorance factor, p, in the weighting expression $w = 4F^2/(\sigma^2(F^2) + (pF^2)^2)^{-1}$	0.06	0.06	0.02
no. of variables	172	145	133
$R_w = [\sum w(\Delta F)^2/\sum wF_{obsd}^2]^{1/2}$	0.064	0.049	0.025
$R = \sum\|\Delta\|/\sum F_{obsd}$	0.081	0.042	0.030
error in observation of unit weight	1.07	1.13	1.04

Three-dimensional Patterson functions showed the positions of the Xe and As atoms. Subsequent least-squares refinements, Fourier calculations, and difference Fourier calculations revealed the fluorine atom positions. Least-squares refinements, in which the function $\sum w(|F_o| - |F_c|)^2/\sum wF_o^2$ was minimized, converged rapidly to the final structures. Scattering factors of Doyle and Turner[15] were used, and anomalous dispersion corrections[16] were applied. The resulting R factors are given in Table I.

Results and Discussion

The fusion temperature versus composition curve for the system XeF_2/XeF_5AsF_6 is given in Figure 1. Points of inflection for the XeF_2:XeF_5AsF_6 combining ratios 1:2 and 1:1 and a maximum at 2:1 indicate adduct formation at these compositions. Crystals of these compounds were obtained and their structures have been determined from X-ray diffraction data. The change in slope of the fusion temperature composition curve in the neighborhood of the composition 3:1 also indicated compound formation, but attempts to secure crystals of that composition were not successful.

The fusion temperature of the $XeF_2 \cdot 2XeF_5AsF_6$ compound is close to 90 °C. Addition of XeF_2 brings about a steep drop in fusion temperature with composition. From approximately 38.5 to 45 mol % XeF_2, in the binary mixture with XeF_5AsF_6, the fusion temperature remains approximately constant at ~61 °C. This composition range spans the XeF_2:XeF_5AsF_6 stoichiometries 2:3 (40%), 3:4 (42.9%), and 4:5 (44.4%) but no convincing crystallographic nor Raman spectroscopic evidence was obtained for any of these possible phases.

The Raman spectra of the three structurally defined phases, with assignments, are given in Figure 2 where they are compared with the spectrum of XeF_5AsF_6. These spectra are essentially the same as those of the earlier study[9] with the spectrum of the 2:1 compound $(XeF_2)_2XeF_5AsF_6$ added. The Xe–F stretching features of that compound, at 420, 438, 479, 542, and 550 cm^{-1}, immediately indicate that the XeF_2 ligands in the 2:1 compound, like that of the 1:1 compound, must be distorted from the $D_{\infty h}$ (idealized) geometry. For XeF_2 in the 1:2 compound, or in XeF_2 (crystalline) itself,[11] the Xe–F stretching is represented by a single intense band at or near 496 cm^{-1}.

The Raman spectra of solids at the compositions 2:3; 3:4, 4:5, and 5:6 did not give clear indication of discrete phases having these compositions. All spectra in that range had the appearance of mixtures of the 1:2 and 1:1 compounds.

Because of the change in slope of the fusion temperature composition curve at the 3:1 composition a more thorough search for compound formation was made at that composition. Raman spectra, shown in Figure 3, were obtained (A) for the melt at 80 °C, (B) for the solid, immediately after solidification of the melt, and (C) for the solid at ~20 °C. From a comparison of the last with the spectrum of $(XeF_2)_2XeF_5AsF_6$, given in Figure 2, it is evident that the 3:1 material is merely a mixture of the 2:1 compound and XeF_2 (the latter giving rise to the 496-cm^{-1} band). The Raman spectrum of the 3:1 composition solid immediately after solidification of the melt (spectrum B) does, however, differ from that at 20 °C and could signify a structural rearrangement toward a material in which the XeF_5^+ is coordinated by three XeF_2 molecules rather than the two XeF_2 and one AsF_6^- of the 20 °C solid. The shift of the XeF stretch in the higher temperature solid at 496 cm^{-1} (which signifies undistorted XeF_2) to 506 and ~462 cm^{-1} (spectrum A) in the melt could mean that all of the XeF_2 is unsymmetrically attached to XeF_5^+ at or near the fusion temperature.

The chemically significant atomic arrangements from the 1:2; 1:1, and 2:1 structural analyses are illustrated in Figures 4, 5, and

(15) Doyle, P. A.; Turner, P. S. *Acta Crystallogr. Sect. A.* **1968**, *24*, 390.
(16) Cromer, D. T.; Liberman, D. *J. Chem. Phys.* **1970**, *53*, 1891.

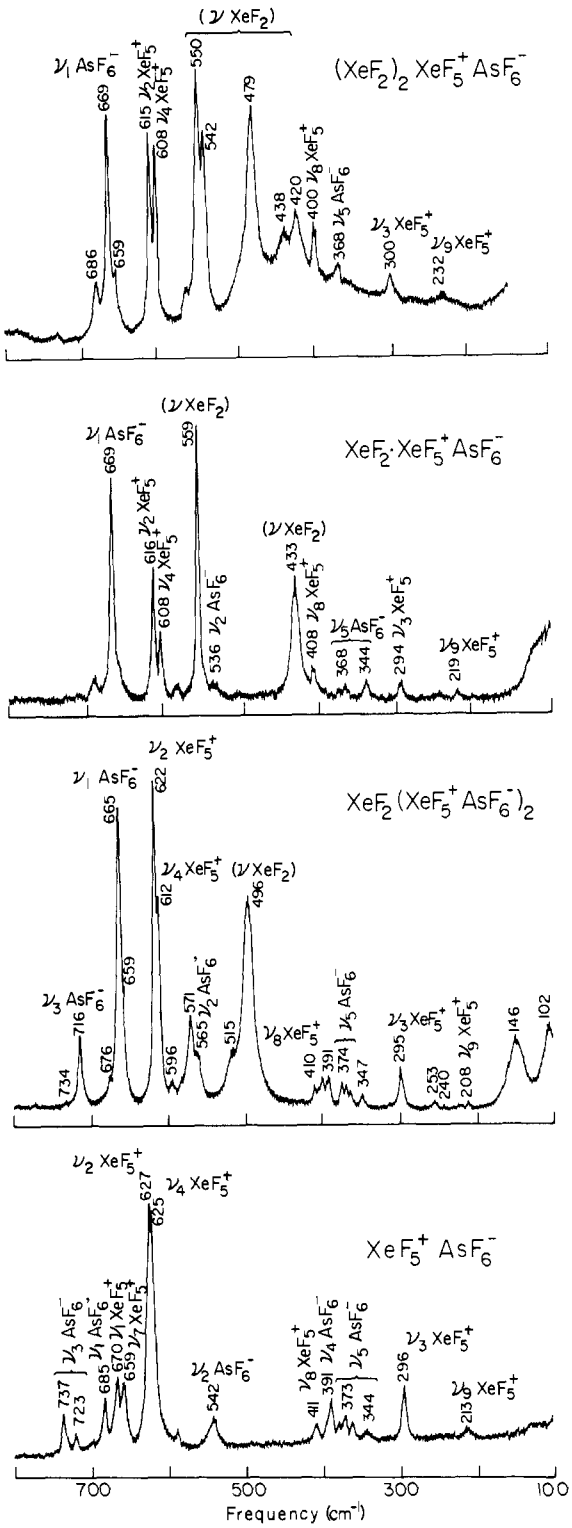

Figure 2. Raman spectra of the 2:1, 1:1, and 1:2 XeF_2/XeF_5AsF_6 compounds and XeF_5AsF_6.

6. Positional parameters for all three structures are given in Table II, and lists of distances and angles are given in Tables III and IV. Thermal parameters are available in the supplementary material.

The coordination of the XeF_5^+ cation by fluorine ligands is variable. The three structures in the present study illustrate this, but similar observations have been made previously.[17] All known coordination geometries for this cation fit the conception of it as a square-pyramidal species (essentially of C_{4v} symmetry) with positive charge centered effectively at the xenon atom. This charge is shielded not only by the five fluorine ligands but also by the formally nonbonding xenon valence electron pair. This electron

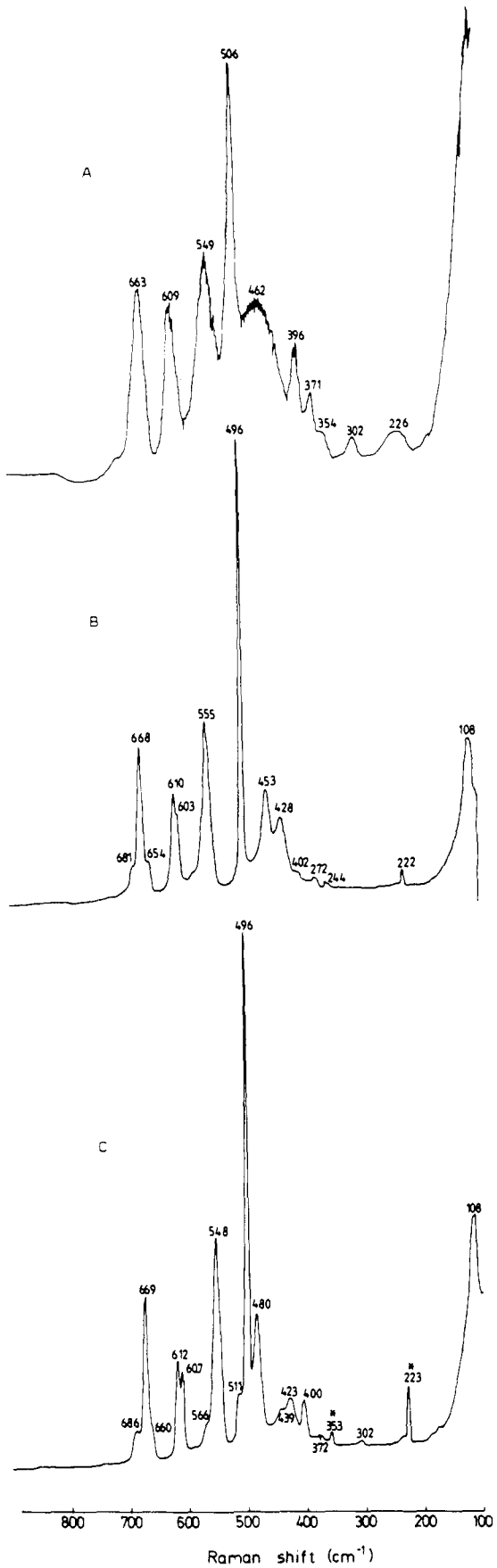

Figure 3. Raman spectra of 3:1 XeF_2/XeF_5AsF_6 (A, melt at ~80 °C; B, solid at ~70 °C; C, solid at ~20 °C).

(17) Leary, K.; Templeton, D. H.; Zalkin, A.; Bartlett, N. *Inorg. Chem.* **1973**, *12*, 1726.

Table II. Positional Parameters[a]

atom	x	y	z
	$2(XeF_2)\cdot XeF_5^+\cdot AsF_6^-$		
Xe(1)	0.19818 (9)	0.0925 (2)	0.09060 (9)
Xe(2)	0.45919 (9)	0.0973 (2)	0.8335 (1)
Xe(3)	0.6885 (1)	0.0757 (2)	0.6136 (1)
As	0.8880 (2)	0.0582 (3)	0.2514 (2)
F(1)	0.599 (1)	−0.080 (2)	0.5532 (9)
F(2)	0.7901 (9)	−0.084 (2)	0.639 (1)
F(3)	0.8015 (9)	0.222 (2)	0.632 (1)
F(4)	0.602 (1)	0.229 (2)	0.5462 (9)
F(5)	0.743 (1)	0.064 (2)	0.494 (1)
F(6)	0.5130 (8)	0.070 (1)	0.6960 (8)
F(7)	0.406 (1)	0.128 (2)	0.965 (1)
F(8)	0.2590 (9)	−0.064 (2)	0.1990 (8)
F(9)	0.146 (1)	0.248 (2)	−0.011 (1)
F(10)	0.763 (1)	0.091 (2)	0.289 (2)
F(11)	0.937 (1)	0.063 (2)	0.375 (1)
F(12)	0.908 (2)	0.257 (2)	0.239 (1)
F(13)	0.826 (2)	0.052 (2)	0.134 (1)
F(14)	0.856 (1)	−0.145 (2)	0.261 (1)
F(15)	1.005 (1)	−0.001 (3)	0.223 (2)
	$XeF_2\cdot XeF_5^+\cdot AsF_6^-$		
Xe(1)	0.5986 (1)	0.3278 (1)	−0.0564 (1)
Xe(2)	0.2044 (2)	0.2109 (1)	0.0355 (1)
As	0.3226 (2)	−0.0240 (2)	−0.2085 (2)
F(1)	0.768 (2)	0.320 (2)	−0.117 (1)
F(2)	0.420 (1)	0.342 (1)	0.0117 (8)
F(3)	0.055 (2)	0.207 (2)	0.104 (1)
F(4)	0.137 (2)	0.382 (1)	0.014 (1)
F(5)	0.317 (2)	0.255 (1)	0.177 (1)
F(6)	0.218 (1)	0.037 (1)	0.078 (1)
F(7)	0.041 (1)	0.163 (1)	−0.085 (1)
F(8)	0.320 (1)	0.101 (1)	−0.1096 (8)
F(9)	0.168 (2)	0.047 (1)	−0.299 (1)
F(10)	0.328 (2)	−0.148 (1)	−0.304 (1)
F(11)	0.479 (1)	−0.093 (1)	−0.112 (1)
F(12)	0.446 (2)	0.068 (1)	−0.254 (1)
F(13)	0.203 (1)	−0.112 (1)	−0.152 (1)
	$XeF_2\cdot 2(XeF_5^+\cdot AsF_6^-)$		
Xe(1)	0.500	0.500	0.500
Xe(2)	0.2332 (1)	0.0673 (2)	0.5454 (1)
As	0.4351 (1)	0.0181 (3)	0.2655 (2)
F(1)	0.3674 (9)	0.386 (1)	0.5719 (9)
F(2)	0.1019 (7)	−0.018 (1)	0.5903 (9)
F(3)	0.2632 (8)	−0.186 (1)	0.557 (1)
F(4)	0.1598 (9)	0.291 (1)	0.5444 (8)
F(5)	0.1597 (8)	0.018 (1)	0.3955 (8)
F(6)	0.2596 (8)	0.093 (1)	0.7125 (7)
F(7)	0.5080 (8)	−0.108 (2)	0.170 (1)
F(8)	0.5469 (8)	0.001 (1)	0.3783 (8)
F(9)	0.3642 (8)	0.144 (1)	0.3694 (9)
F(10)	0.492 (1)	0.221 (1)	0.226 (1)
F(11)	0.324 (1)	0.037 (2)	0.1651 (9)
F(12)	0.381 (1)	−0.173 (2)	0.323 (1)

[a] Here and in the following tables the number in parentheses is the estimated standard deviation for the least significant figures.

pair is visualized as occupying the sixth coordination site of the pseudooctahedral cation. In harmony with this picture, fluorine ligands of molecules or ions which make close approach to XeF_5^+ do so at an angle of ~50 °C to the fourfold axis on which the electron pair is deemed to be concentrated. These ligands, two or three, as here, but in other structures four in number, are generally distributed to maximize their mutual separation. All of this fits the notion of a discrete cation, attracting ligands of other species electrostatically.

The $XeF_2\cdot 2(XeF_5\cdot AsF_6)$ structure is shown in Figure 4. The xenon difluoride molecule, which is centered on a center of symmetry, has an Xe–F interatomic distance of 2.01 (1) Å (2.03 (1) Å corrected for thermal motion) and is therefore not significantly different from XeF_2 in the crystalline solid[7] where the Xe–F distance is 2.01 (1) Å. This is in harmony with the identity of the symmetric vibration for the XeF_2 in $XeF_2\cdot 2(XeF_5AsF_6)$ at 496 cm^{-1} (see figure 2) with that[11] of crystalline XeF_2 at 496 cm^{-1}.

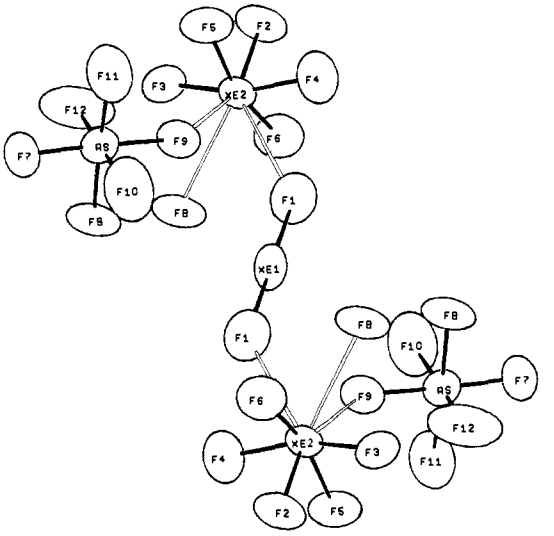

Figure 4. ORTEP drawing of the molecular unit of $XeF_2\cdot 2(XeF_5^+\cdot AsF_6^-)$ with use of 50% probability ellipsoids. Two extra F(8) atoms have been included to show the complete bonding environment of Xe(2).

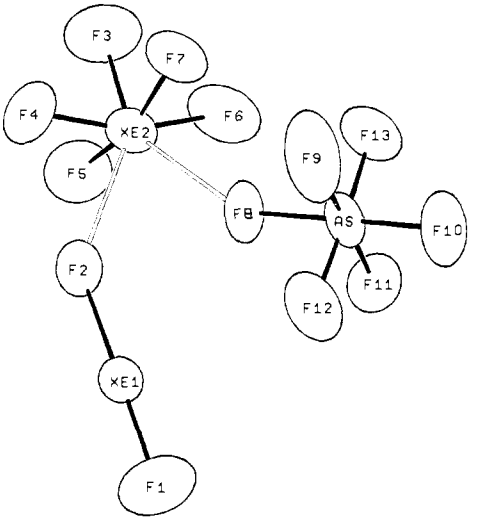

Figure 5. ORTEP drawing of one molecular unit of $XeF_2\cdot XeF_5^+\cdot AsF_6^-$ with use of 50% probability ellipsoids.

The XeF_5 and AsF_6^- species are very similar to their relatives in[13] the parent material, XeF_5AsF_6. The cation is linked to one XeF_2 and two AsF_6^- via F bridges: the XeF_2 at 2.76 (1) Å and the two separate AsF_6^- at 2.66 (1) and 2.74 (1) Å. The coordination of XeF_5^+ in XeF_5AsF_6 is similar. There, two of the bridging F ligands (at 2.73 (2) and 2.83 (2) Å) are cis related fluorine atoms of one AsF_6^-, and the other (at 2.65 (2) Å) is contributed by a second AsF_6^-. By this arrangement two formula units in XeF_5AsF_6 are related by a center of symmetry and form a molecular unit which is also the structural unit. When XeF_5AsF_6 is melted, the liquid is mobile. This is in sharp contrast to the viscous melt given by $XeF_2\cdot 2(XeF_5AsF_6)$. The XeF_2 molecule, by its bridging interaction with the two XeF_5^+, contributes to the polymeric nature of the $XeF_2\cdot 2(XeF_5AsF_6)$ material. This polymeric nature also derives from the bridge bonds that each cation makes to two separate AsF_6^-. Each AsF_6^- in turn is linked to two XeF_5^+ to generate an extended three-dimensional network. Evidently the interaction between the various species in the crystal must be largely retained in the melt close to the melting point, since the Raman spectra of solid and melt are similar.

When the 1:2 phase is enriched with XeF_2 the only new phase observed, up to the composition 1:1, is the phase with the latter composition. This has the structure illustrated in Figure 5. Both the XeF_2 and the XeF_5^+ are differently coordinated from their situations in $XeF_2\cdot 2XeF_5AsF_6$. a one-on-one interaction of XeF_2 with XeF_5^+ is preferred in the 1:1 compound. This evidently is

Table III. Interatomic Distances[a]

$2(XeF_2)\cdot XeF_5^+\cdot AsF_6^-$			$XeF_2\cdot XeF_5^+\cdot AsF_6^-$			$XeF_2\cdot 2(XeF_5^+\cdot AsF_6^-)$		
atoms	D (Å)	corr[b]	atoms	D (Å)	corr[b]	atoms	D (Å)	corr[b]
Xe(1)–F(9)	1.94	1.99	Xe(1)–F(1)	1.91	1.97			
Xe(2)–F(7)	1.96	2.01						
Xe(1)–F(8)[c]	2.04	2.05	Xe(1)–F(2)[c]	2.05	2.06	Xe(1)–2F(1)[c]	2.01	2.03
Xe(2)–F(6)[c]	2.04	2.05						
Xe(3)–F(1)	1.83	1.86	Xe(2)–F(3)	1.80	1.84	Xe(2)–F(2)	1.80	1.83
Xe(3)–F(2)	1.83	1.86	Xe(2)–F(4)	1.84	1.88	Xe(2)–F(3)	1.81	1.84
Xe(3)–F(3)	1.84	1.87	Xe(2)–F(5)	1.82	1.85	Xe(2)–F(4)	1.80	1.83
Xe(3)–F(4)	1.83	1.86	Xe(2)–F(6)	1.83	1.87	Xe(2)–F(5)	1.82	1.85
Xe(3)–F(5)	1.81	1.86	Xe(2)–F(7)	1.85	1.88	Xe(2)–F(6)	1.83	1.86
Xe(3)–F(6)[c]	2.52		Xe(2)–F(2)[c]	2.47		Xe(2)–F(1)[c]	2.76	
Xe(3)–F(8)[c]	2.54		Xe(2)–F(8)[c]	2.59		Xe(2)–F(8)[c]	2.74	
Xe(3)–F(14)[c]	2.94					Xe(2)–F(9)[c]	2.66	
As–F(10)	1.68	1.75	As–F(8)[c]	1.77	1.79	As–F(7)	1.68	1.72
As–F(11)	1.71	1.78	As–F(9)	1.69	1.77	As–F(8)[c]	1.74	1.78
As–F(12)	1.68	1.76	As–F(10)	1.74	1.78	As–F(9)[c]	1.73	1.76
As–F(13)	1.69	1.79	As–F(11)	1.73	1.75	As–F(10)	1.65	1.71
As–F(14)[c]	1.74	1.77	As–F(12)	1.68	1.73	As–F(11)	1.65	1.72
As–F(15)	1.60	1.74	As–F(13)	1.71	1.75	As–F(12)	1.65	1.73

[a] Estimated standard deviations are all between 0.01 and 0.02 Å. [b] Corrected for thermal motion assuming the light atom "rides" on the heavy atom. [c] Bridging fluorine atoms.

Table IV. Selected Bond Angles[a]

$2(XeF_2)\cdot XeF_5^+\cdot AsF_6^-$		$XeF_2\cdot XeF_5^+\cdot AsF_6^-$		$XeF_2\cdot 2(XeF_5^+\cdot AsF_6^-)$	
F(8)–Xe(1)–F(9)	177	F(1)–Xe(1)–F(2)	178	F(1)–Xe(1)–F(1)	180[b]
F(6)–Xe(2)–F(7)	179				
F(5)–Xe(3)–F(1)	80	F(3)–Xe(2)–F(4)	80	F(2)–Xe(2)–F(3)	80
F(5)–Xe(3)–F(2)	80	F(3)–Xe(2)–F(5)	81	F(2)–Xe(2)–F(4)	81
F(5)–Xe(3)–F(3)	79	F(3)–Xe(2)–F(6)	81	F(2)–Xe(2)–F(5)	80
F(5)–Xe(3)–F(4)	81	F(3)–Xe(2)–F(7)	80	F(2)–Xe(2)–F(6)	80
F(1)–Xe(3)–F(2)	87	F(4)–Xe(2)–F(5)	89	F(3)–Xe(2)–F(5)	87
F(2)–Xe(3)–F(3)	88	F(5)–Xe(2)–F(6)	89	F(5)–Xe(2)–F(4)	88
F(3)–Xe(3)–F(4)	90	F(6)–Xe(2)–F(7)	87	F(4)–Xe(2)–F(6)	88
F(4)–Xe(3)–F(1)	89	F(7)–Xe(2)–F(4)	88	F(6)–Xe(2)–F(3)	91
F(1)–Xe(3)–F(3)	159	F(4)–Xe(2)–F(6)	161	F(3)–Xe(2)–F(4)	162
F(2)–Xe(3)–F(4)	161	F(5)–Xe(2)–F(7)	161	F(5)–Xe(2)–F(6)	160
F(10)–As–F(11)	87	F(8)–As–F(9)	89	F(7)–As–F(8)	89
F(10)–As–F(12)	91	F(8)–As–F(11)	89	F(7)–As–F(10)	92
F(10)–As–F(13)	87	F(8)–As–F(12)	89	F(7)–As–F(11)	94
F(10)–As–F(14)	85	F(8)–As–F(13)	87	F(7)–As–F(12)	93
F(11)–As–F(12)	92	F(9)–As–F(10)	92	F(8)–As–F(9)	88
F(11)–As–F(14)	91	F(9)–As–F(12)	93	F(8)–As–F(10)	86
F(11)–As–F(15)	90	F(9)–As–F(13)	89	F(8)–As–F(12)	89
F(12)–As–F(13)	90	F(10)–As–F(11)	90	F(9)–As–F(10)	88
F(12)–As–F(15)	98	F(10)–As–F(12)	91	F(9)–As–F(11)	89
F(13)–As–F(14)	87	F(10)–As–F(13)	93	F(9)–As–F(12)	86
F(13)–As–F(15)	96	F(11)–As–F(12)	88	F(10)–As–F(11)	95
F(14)–As–F(15)	86	F(11)–As–F(13)	90	F(11)–As–F(12)	90
F(10)–As–F(15)	171	F(8)–As–F(10)	179	F(7)–As–F(9)	177
F(11)–As–F(13)	174	F(9)–As–F(11)	178	F(8)–As–F(11)	177
F(12)–As–F(14)	175	F(12)–As–F(13)	176	F(10)–As–F(12)	172
Xe(3)–F(8)–Xe(1)	141	Xe(2)–F(2)–Xe(1)	140	Xe(2)–F(1)–Xe(1)	140
Xe(3)–F(6)–Xe(2)	140	Xe(2)–F(8)–As	152	Xe(2)–F(8)–As	152
Xe(3)–F(14)–As	149			Xe(2)–F(9)–As	137
F(5)–Xe(3)–F(6)	143	F(2)–Xe(2)–F(3)	144	F(1)–Xe(2)–F(8)	65
F(5)–Xe(3)–F(8)	144	F(3)–Xe(2)–F(8)	147	F(1)–Xe(2)–F(9)	62
F(6)–Xe(3)–F(8)	73	F(2)–Xe(2)–F(8)	69	F(8)–Xe(2)–F(9)	69

[a] Estimated standard deviations for all angles are ±1°. [b] Angle is 180° by symmetry.

associated with both the distortion of the linear XeF_2 and the lowering of the coordination number of the XeF_5^+, from three bridging F ligands in the 1:2 compound (2.66 (2), 2.74 (2), and 2.76 (2) Å) to two in the 1:1 compound (2.47 (2) and 2.59 (2) Å).

These structural changes must be a consequence of the easy transition of the semi-ionic symmetrical F–Xe–F toward the ion pair $(F–Xe)^+F^-$. In the symmetrical electrostatic field provided by the structural arrangement in the 1:2 compound, the XeF_2 is indistinguishable from XeF_2 in the crystalline solid. But in the unsymmetrical field of the single XeF_5^+ of the 1:1 compound the progression toward ionization is easily perceived, both in the observed interatomic distances and in the vibrational spectra. The diminished coordination number of the XeF_5^+ in the 1:1 compound must be a consequence of the high charge on the bridging F ligand of the XeF_2. That high charge brings it closer to the XeF_5^+ and screens that cation charge more effectively while simultaneously repelling other negatively charged ligands. Thus the coordination of the XeF_5^+ by only two F ligands is easily understood. As a consequence of these strong linkages of the XeF_5^+ to the XeF_2 and the AsF_6^-, the formula unit represents a discrete structural unit. This "molecular" structure accounts for the higher mobility of the melt, which contrasts with the viscous one obtained on melting the 1:2 compound.

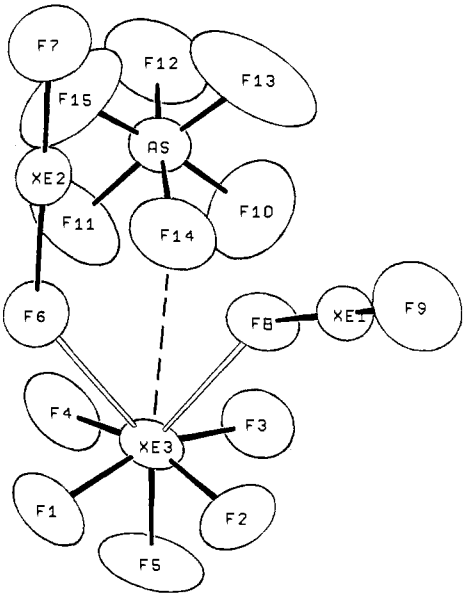

Figure 6. ORTEP drawing of the molecular unit of $2XeF_2 \cdot (XeF_5^+ \cdot AsF_6^-)$ with use of 50% probability ellipsoids.

It is of interest that the 1:1 structure has the form shown, rather than the polymeric form ··FXeF··XeF_5^+··FXeF·· with symmetrical XeF_2 and three coordinated XeF_5^+, as in the 1:2 compound (the AsF_6^- would complete the XeF_5^+ coordination). Presumably the bonding energy for the polymeric form, if better than for the monomer, is insufficiently superior to offset the disadvantageous entropy of the polymer, relative to the monomer. It must be supposed that the polymeric 1:2 structure occurs because the binding of symmetrical XeF_2 to XeF_5^+ is energetically better than the binding of a second F ligand of AsF_6^- (the XeF_5^+ is coordinated by one F ligand of one anion and two of a second in XeF_5AsF_6). Clearly, however, the 1:1 "molecular" structure with its partially ionized XeF_2 does not persist in the presence of XeF_5AsF_6. Evidently in that situation the XeF_5^+ captures the remaining F ligand of the partially ionized XeF_2 of the 1:1 compound and produces the symmetrically bridged 1:2 polymer.

The structure of the 2:1 compound, shown in Figure 6, is entirely consistent with the coordination character seen in the other structures. Here, as in the 1:1 compound, the XeF_2 is coordinated singly by the XeF_5^+ species. As is appropriate for the 2:1 stoichiometry, each XeF_5^+ has two XeF_2 molecules coordinated via short Xe···F bridges of 2.53 (1) and 2.54 (1) Å. The XeF_5^+ coordination is indeed similar to that of the 1:1 compound with the coordinated AsF_6^- of that arrangement having been replaced by the second XeF_2 molecule. The bridging F ligands of the two XeF_2 molecules, the Xe(VI) atom and its axial F ligand (F5), lie in the same plane (the sum of angles F(6)–Xe(3)–F(8), F(6)–Xe(3)–F(5), and F(8)–Xe(3)–F(5) is 359.4 (17)°). It therefore appears that the $Xe(VI)^+ \cdots FAsF_5^-$ interatomic distance of 2.94 (1) Å represents merely a secondary close-packing interaction, that fluorine ligand not being part of the primary coordination sphere of the cation. Although the two XeF_2 molecules coordinated to the XeF_5^+ in the 2:1 compound are not crystallographically equivalent they are not significantly different in their interatomic distances and orientation with respect to the cation. The XeF_2 molecules do not interact as strongly with the XeF_5^+ in this 2:1 complex as does the XeF_2 in the 1:1 compound. This is expressed not only in the shorter Xe(VI)···F distance in the 1:1 versus the 2:1 compound (2.47 (1) versus 2.53 (1) Å) but in the greater distortion in the former relative to the latter (2.06 (1) with 1.97 (1) Å versus 2.05 (1) with 1.99 (1) or 2.01 (1) Å). This may simply be a consequence of the mutual repulsion of the two XeF_2 ligands of the cation in the 2:1 compound being greater than the repulsive interaction of the single XeF_2 and the coordinated AsF_6 ion. Indeed the two XeF_2 molecules coordinated to the cation in the 2:1 compound are so coordinated (as can be seen from figure 6) that the two xenon atoms (each positively charged) are well separated from one another. Clearly the formula unit $2XeF_2 \cdot XeF_5AsF_6$ forms a discrete unit. Like the melt of the 1:1 compounds, that of the 2:1 compounds is much more mobile than that given by the 1:2 material; moreover the eutectic between the "molecular" 1:1 and 2:1 materials provides the lowest fusion temperature in this system. This, and compositionally close melts, readily supercool to room temperatures.

Table V. Interatomic Distances, Vibrational Frequencies, and Force Constants for XeF_2 and Linearly Distorted XeF_2 Species

compd	F–Xe dist[a] (Å)	Xe···F dist[a] (Å)	XeF stretching modes (cm^{-1})	force constants[b] (mdyn/(Å)) k_1	k_2
$F \cdot XeF \cdot Sb_2F_{10}$	1.82 (3)	2.34 (3)[c]	620, 269[d-f]	3.76	0.72
$F \cdot XeFAsF_5$	[1.94 (1)]	[2.25 (1)][g]	609, 346[d,g]	3.63	1.19
	1.873 (6)	2.212 (5)			
$Xe_2F_3AsF_6$	1.90 (3)	2.14 (3)[h]	600, 401[d,e]	3.43	1.67
XeF_2	[2.01 (1)][i]		547, 496[j]		
	1.984 (4)				
$XeF_2 \cdot 2XeF_5AsF_6$	[2.03 (1)]		~547, 496		
	2.01 (1)				
$XeF_2 \cdot XeF_5AsF_6$	[1.97 (1)]	[2.06 (1)]	559, 433	3.02	1.89
	1.91 (1)	2.05 (1)			
	2.68				
	2.68				

[a] Interatomic distances given within square brackets are distances corrected for the riding motion of the F atom on the Xe atom. [b] The force constants were evaluated following Herzberg[28] with $\lambda_1 + \lambda_3 = \mu_F(k_1 + k_2) + \mu_{Xe}(k_1 + k_2 - 2k_{12})$ and $\lambda_1\lambda_3 = (k_1k_2 - k_{12}^2)(\mu_F^2 + 2\mu_F\mu_{Xe})$; $\lambda_2 = 4\pi^2c^2\nu_i^2$ and μ_i reciprocal atomic masses. The k_{12} for XeF_2 was used for the other cases. [c] Reference 20. [d] Reference 26. [e] Reference 21. [f] Reference 27. [g] Reference 18. [h] Reference 13. [i] Reference 23. [j] Reference 11.

The XeF_2 molecules seen in the present structures conform to the now well documented pattern of Xe(II) linearly coordinated by only two F ligands. The distortions from centrosymmetry, seen in the $XeF_2 \cdot XeF_5AsF_6$ and the $(XeF_2)_2XeF_5AsF_6$ structure, are less extreme versions of the distortions previously described for XeF_2 coordinated to strong fluoride ion acceptors. Table V gives the essential dimensions and vibrational data that characterize these linearly distorted F—Xe···F systems. Undistorted XeF_2 data are included for comparison purposes. All observations are compatible with linearly coordinated Xe(II) with one F ligand departing on the F—Xe—F → F—Xe^+···F^- ionization pathway toward the XeF_5^+ cation. The situation is related to that observed in the 1:1 complexes (roughly formulated as $XeF^+MF_6^-$) which XeF_2 makes with strong fluoride ion acceptors[18-20] (e.g., M = As, Ru, Sb) and that which occurs[13] in the complex cation $Xe_2F_3^+$. These geometries are compared in Table V. In all cases the lengthening of one Xe–F bond is accompanied by the contraction of the other. Evidently the canonical form $\{(F\text{–}Xe)^+F^-(XeF_5)^+\}$ is more important than $\{F^-(Xe\text{–}F)^+(XeF_5)^+\}$. The weakening of one bond of the XeF_2 and the strengthening of the other is indicated by the vibrational data. Vibrational aspects of XeF_2 complexes with fluoride ion acceptors have been discussed previously.[21,22]

From the data on FXeF species in Table V the most distorted (and ionized) form is seen to be that in the compound[20] $FXeF\text{-}Sb_2F_{10}$. Although the interatomic distances in the crystal are imprecise [Xe–F = 1.82 (3) and 2.34 (3) Å], the vibrational data clearly indicate the greatest force constant differences for any

(18) Zalkin, A.; Ward, D. L.; Biagioni, R. N.; Templeton, D. H.; Bartlett, N. *Inorg. Chem.* **1978**, *17*, 1318.
(19) Bartlett, N.; Gennis, M.; Gibler, D. D.; Morrell, B. K.; Zalkin, A. *Inorg. Chem.* **1973**, *12*, 1717.
(20) Burgess, J.; Fraser, C. J. W.; McRae, V. M.; Peacock, R. D.; Russell, D. R. *Inorg. Nucl. Chem.—Herbert H. Hyman Mem. Vol.* **1976**, 183.
(21) Sladky, F. O.; Bulliner, P. A.; Bartlett, N. *J. Chem. Soc. A* **1969**, 2179.
(22) Frlec, B.; Holloway, J. H. *J. Chem. Soc., Dalton Trans.* **1975**, 535.

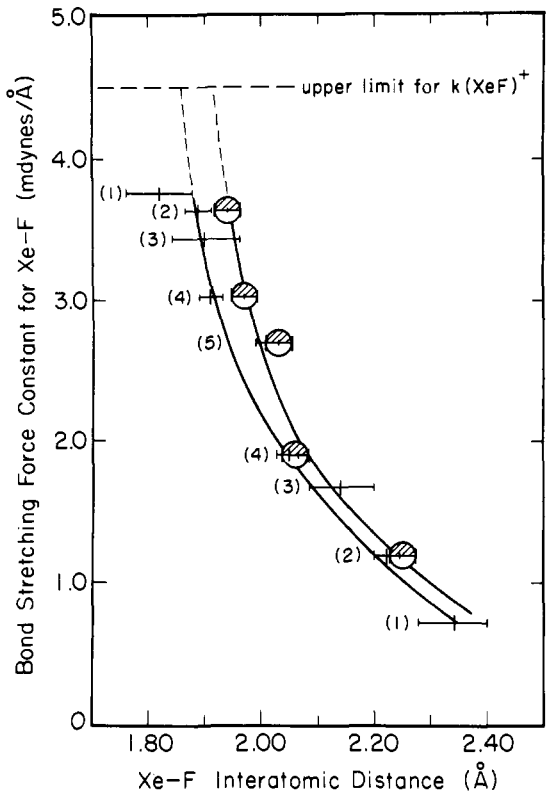

Figure 7. Force constant–interatomic distance relationships for XeF_2 species (⊖, distances corrected for the riding of F on Xe; —|—, uncorrected distances): (1) $FXeFSb_2F_{10}$, (2) $FXeFAsF_5$, (3) $Xe_2F_3AsF_6$, (4) $XeF_2{\cdot}XeF_5AsF_6$, and (5) $XeF_2{\cdot}2XeF_5AsF_6$.

linearly distorted FXeF species, that for the shorter bond being 3.76 and the larger 0.72 mdyn/Å. These values together with the force constant for the bonds in the symmetrical XeF_2, which is 2.68 mdyn/Å, provide a basis for assessing the charge distribution in the XeF_2/XeF_5^+ complexes.

Since the XeF_2 in the $XeF_2{\cdot}2(XeF_5AsF_6)$ compound is indistinguishable dimensionally and vibrationally from crystalline XeF_2,[23] the F ligand charge must be the same. The Jortner et al.[2] value of −0.5e is therefore appropriate. The charge on the longer bonded F ligand in the 1:1 and 2:1 compounds must exceed this. Yet the degree of ionization in these FXeF species is clearly much less than that in the $FXeFSb_2F_{10}$ situation.

From the force constant dependence upon interatomic distance for the linearly distorted FXeF species illustrated in Figure 7, it is seen that the force constant rises sharply as the short bond interatomic distance approaches a limiting value. The sum of the force constants decreases as the distortion increases (see Table V). If this trend continues, as seems likely, to the ionization limit, the force constant for the fully ionized $(Xe–F)^+$ species must be ≤4.48 (i.e., 3.76 + 0.72) mdyn/Å. This suggests an interatomic distance for the cation $(Xe–F)^+$, based on the corrected data of ~1.92 Å. The uncorrected data indicate a somewhat lower cation interatomic distance of ~1.86 Å. Spectroscopic data for the isoelectronic I–F species provide an interatomic distance[24] of 1.908_9 Å. It appears that the $(Xe–F)^+$ distance must be very similar. Clearly the XeF_2 molecules, which are coordinated to only one XeF_5^+, are in the early stages of ionization. In each case the charge on the long-bonded F ligand must be >0.5e (the charge of the undistorted XeF_2 ligand) but ≪1.0e.

In studies related to those of this paper Žemva and his coworkers[25] have shown that the salt XeF_5RuF_6 forms a 1:1 complex with XeF_2 whereas the isostructural relative XeF_5NbF_6 does not. They have also been unable to form XeF_2/XeF_5^+ complexes of salts of dianions. These observations fit the model developed in the rationalization of the XeF_2/XeF_5AsF_6 structures. Clearly the XeF_2 must be capable of displacing F bridges of the anion to the XeF_5^+ in the parent $XeF_5(MF_6)$ structure, if a XeF_2 complex is to exist. In general, the higher the negative charge on each ligand of the anion, the less effective will be the XeF_2 in displacing such a ligand from a bridging interaction with XeF_5^+. Since the ligand charge on MF_6^- must decrease across each transition series (when the formally nonbonding electrons are in t_{2g} orbitals) the ligands of XeF_2 are more likely to displace MF_6^- bridges to XeF_5^+ when M is at or near the end of a transition series. For similar reasons it is unlikely that XeF_2/XeF_5^+ complexes can occur with doubly or triply charged anions.

Acknowledgment. The authors gratefully acknowledge the following support: Preparations and crystallographic studies of the 2:1, 1:1, and 1:2 XeF_2/XeF_5AsF_6 complexes were carried out at Berkeley with the support of the Director, Office of Energy Research, Office of Basic Energy Sciences, Chemical Science Division of the U.S. Department of Energy under Contract No. DE-AC03-67SF00098. One of us (B.Ž.) held a fellowship of the Boris Kidrič Foundation and received travel support from the Senior Fulbright-Hays Program. The full survey of the XeF_2/XeF_5AsF_6 system was carried out with the support of the U. S.–Yugoslav Joint Fund for Scientific and Technological Cooperation, in cooperation with the National Science Foundation under Grant No. 552. That part of the work was also supported by the Research Community of Slovenia.

Supplementary Material Available: Tables of thermal parameters for $2XeF_2{\cdot}XeF_5{\cdot}AsF_6$, $XeF_2{\cdot}XeF_5{\cdot}AsF_6$, and $XeF_2{\cdot}2(XeF_5{\cdot}AsF_6)$ (2 pages); listing of observed and calculated structure factors for $2(XeF_2){\cdot}XeF_5{\cdot}AsF_6$, $XeF_2{\cdot}XeF_5{\cdot}AsF_6$, and $XeF_2{\cdot}2(XeF_5{\cdot}AsF_6)$ (22 pages). Ordering information is given on any current masthead page.

(23) Levy, H. A.; Agron, P. A. In *Noble Gas Compounds*; Hyman, H. H., Ed.; The University of Chicago Press: Chicago and London, 1963; p 221.

(24) *Tables of Constants and Numerical Data, No. 17, Spectroscopic Data Relative to Diatomic Molecules*; Rosen, B., general editor; Pergamon: New York, 1970.

(25) Žemva, B.; Golič, L.; Slivnik, J. *Vestn. Slov. Kem. Drus.* **1983**, *30*, 365.

(26) Gillespie, R. J.; Landa, B. *Inorg. Chem.* **1973**, *12*, 1383.

(27) Chaivanov, B. B. *Russ. J. Phys. Chem.* **1972**, *46*, 13.

(28) Herzberg, G. *Infrared and Raman Spectra*; D. Van Nostrand Co., Inc.: Princeton, NJ, 1964; p 187.